J Neurophysiol 107: 3256–3266, 2012.
First published March 21, 2012; doi:10.1152/jn.01132.2011.

Functional characterization of dI6 interneurons in the neonatal mouse spinal cord

Jason Dyck,[1] Guillermo M. Lanuza,[2] and Simon Gosgnach[1]

[1]*Department of Physiology, Center for Neuroscience, University of Alberta, Edmonton, Alberta, Canada; and* [2]*Fundacion Instituto Leloir, Buenos Aires, Argentina*

Submitted 13 December 2011; accepted in final form 18 March 2012

Dyck J, Lanuza GM, Gosgnach S. Functional characterization of dI6 interneurons in the neonatal mouse spinal cord. *J Neurophysiol* 107: 3256–3266, 2012. First published March 21, 2012; doi:10.1152/jn.01132.2011.—Our understanding of the neural control of locomotion has been greatly enhanced by the ability to identify and manipulate genetically defined populations of interneurons that comprise the locomotor central pattern generator (CPG). To date, the dI6 interneurons are one of the few populations that settle in the ventral region of the postnatal spinal cord that have not been investigated. In the present study, we utilized a novel transgenic mouse line to electrophysiologically characterize dI6 interneurons located close to the central canal and study their function during fictive locomotion. The majority of dI6 cells investigated were found to be rhythmically active during fictive locomotion and could be divided into two electrophysiologically distinct populations of interneurons. The first population fired rhythmic trains of action potentials that were loosely coupled to ventral root output and contained several intrinsic membrane properties of rhythm-generating neurons, raising the possibility that these cells may be involved in the generation of rhythmic activity in the locomotor CPG. The second population fired rhythmic trains of action potentials that were tightly coupled to ventral root output and lacked intrinsic oscillatory mechanisms, indicating that these neurons may be driven by a rhythm-generating network. Together these results indicate that dI6 neurons comprise an important component of the locomotor CPG that participate in multiple facets of motor behavior.

central pattern generator; neural circuit

ALTERNATING RHYTHMIC ACTIVITY in hindlimb muscles during locomotion is generated by a neural network referred to as the locomotor central pattern generator (CPG), which is located in the ventro-medial region of the lower thoracic and lumbar spinal cord. Because of its distributed nature (Cowley and Schmidt 1997; Kjaerulff and Kiehn 1996), traditional anatomical and electrophysiological experiments have proven to be of limited use for the identification of the structure and function of the locomotor CPG (Kiehn 2006). Recently, a molecular approach has been used to identify five classes of interneurons that are located in the ventral spinal cord postnatally (dI6, V0–V3). Many of these can be identified by expression of a unique complement of transcription factors at early embryonic time points and can be further divided into subpopulations based on downstream transcription factor expression (Goulding 2009).

Address for reprint requests and other correspondence: S. Gosgnach, Dept. of Physiology, Center for Neuroscience, Univ. of Alberta, 7-47 Medical Science Bldg., Edmonton, AB, T6G 2H7, Canada (e-mail: gosgnach@ualberta.ca).

Initial experiments have demonstrated that several of these genetically defined cell populations play specific roles in the production of locomotor behavior. Clear deficits in the fictive locomotor pattern have been observed in the absence of the V0 (Lanuza et al. 2004) and V1 (Gosgnach et al. 2006) populations, and subsequent experiments have demonstrated changes in the fictive locomotor pattern when the V2a (Crone et al. 2008, 2009; Zhong et al. 2010) and V3 (Zhang et al. 2008) populations are ablated or silenced. Whole cell recordings of intrinsic membrane properties carried out on several populations have provided further insight into their physiological role during locomotor activity (Dougherty and Kiehn 2010; Lundfald et al. 2007; Zhang et al. 2008; Zhong et al. 2010).

One population of cells that have been suggested to play a role during locomotor activity, but have yet to be directly investigated, are the dI6 interneurons (Lanuza et al. 2004). These cells originate from progenitors immediately dorsal to the p0 domain and migrate ventro-medially during embryogenesis, taking up positions in laminae VII/VIII of the postnatal spinal cord (Gross et al. 2002). While these cells, together with the dI1–dI5 populations, have been shown to express Lbx1 at early embryonic time points, the lack of a unique molecular marker for the dI6 population has hindered their functional characterization. Interestingly, these cells share many similarities with the V0 interneurons, which originate immediately ventral to the dI6 cells, arise from Dbx1 progenitors, do not express Lbx1, and can be divided into a ventral subpopulation that expresses Evx1/2 and a dorsal subpopulation that does not. In addition to having a similar migration pattern, both the dI6 and the dorsal subset of V0 cells develop from Pax7 and Dbx2 progenitors. Furthermore, in the Dbx1 mutant mouse, many V0 neurons acquire characteristics of dI6 cells soon after their generation. This has led to the suggestion that the dI6 population may play a complementary role to the V0 cells during locomotion (Goulding 2009; Lanuza et al. 2004; Rabe et al. 2009); however, this hypothesis has yet to be tested.

In this study we utilize a transgenic mouse model that allows for identification of a subset of the dI6 cells located in the proximity of the central canal via differential expression of reporter proteins. An investigation of their intrinsic membrane properties as well as their activity during fictive locomotion demonstrates that there are two, electrophysiologically distinct, populations of dI6 interneurons that are rhythmically active during fictive locomotion. The first have properties consistent with cells that coordinate motoneuron output during locomotion. The second have several electrophysiological characteristics of oscillatory cells and may be involved in generating rhythmicity in the locomotor CPG.

MATERIALS AND METHODS

Animals. All procedures were in accordance with the Canadian Council on Animal Care (CCAC) and approved by the Animal Welfare Committee at the University of Alberta. For generation of the $Dbx1^{Cre}$ transgenic mouse, sequences encoding for Cre recombinase, including a nuclear localization signal and SV40 polyadenylation sequence, were inserted downstream of a 5.7-kb Dbx1 genomic DNA fragment (a gift from Frank Ruddle; Lu et al. 1996). The Dbx1 promoter-Cre construct was flanked by chicken β-globin insulators (Chung et al. 1993) and linearized for pronuclear injection. Potential founder mice were genotyped for Cre by PCR using specific oligonucleotide primers as described previously (Gosgnach et al. 2006; Lanuza et al. 2004).

In total, electrophysiological and immunohistochemical experiments were performed on 63 male and female embryonic (E10–E12) and neonatal (0–3 days of age) mice. Initially $Dbx1^{Cre}$ mice were mated with $Rosa26^{EGFP}$ and $Rosa26^{EYFP}$ reporter lines (acquired from The Jackson Laboratory and collectively referred to as $Rosa26^{EFP}$) as well as $Dbx1^{LacZ}$ mice (Pierani et al. 2001) to assess specific Cre-mediated recombination (see Fig. 1). After it was determined that the dI6 population could be visually identified in $Dbx1^{Cre}$; $Rosa26^{EFP}$ mice via reporter protein expression, $Dbx1^{Cre}$; $Rosa26^{EFP}$ or $Dbx1^{Cre}$; $Rosa26^{EFP}$; $Dbx1^{LacZ}$ offspring were used for electrophysiological experiments.

In vitro preparation. Mice were anesthetized via inhalation of isoflurane (4% delivered with 95% O_2-5% CO_2). After decapitation and evisceration, the spinal cord was dissected out in a bath containing oxygenated, ice-cold dissecting artificial cerebrospinal fluid (d-aCSF) with low Ca^{2+} and high Mg^{2+} concentrations. This solution contained (in mM) 111 NaCl, 3.08 KCl, 11 glucose, 25 $NaHCO_3$, 1.18 KH_2PO_4, 3.7 $MgSO_4$, and 0.25 $CaCl_2$ (pH 7.4, osmolarity 280–300 mosM). The preparation used for targeting interneurons located close to the central canal for whole cell recording in the mouse spinal cord has been described in detail previously (Dyck and Gosgnach 2009). Briefly, the spinal cord was transferred to a vibratome chamber containing oxygenated d-aCSF and glued, dorsal side up, to a strip of agarose. The vibratome was then used to shave away sections of the dorsal aspect of the lumbar spinal cord until the central canal was visible with a dissecting microscope. After sectioning, the spinal cord was situated dorsal side up on a coverslip in a Plexiglas recording chamber and held in place via nylon threads stretched over a platinum wire flattened into a horseshoe shape.

Electrophysiological recording. The preparation was constantly perfused with room-temperature, oxygenated recording artificial cerebrospinal fluid (r-aCSF) that was identical to the dissecting solution except for the following (in mM): 1.25 $MgSO_4$, 2.52 $CaCl_2$. In all experiments fictive locomotor activity was induced by bath application of 10 μM 5-hydroxytryptamine (5-HT) and 5 μM *N*-methyl-D-aspartate (NMDA) (both from Sigma-Aldrich) and monitored via electroneurogram (ENG) activity recorded from bipolar suction electrodes (A-M Systems) positioned on the flexor-related (second lumbar, i.e., L2) and/or extensor-related (fifth lumbar, i.e., L5) ventral roots. ENG signals were amplified ($\times$20,000) and band-pass filtered (100 Hz–1 kHz) with custom-made equipment (R&R Designs). All ENG, as well as whole cell, data were digitized (Digidata 1440A, Axon Instruments) and recorded with pCLAMP software (Axon Instruments) on a PC.

For whole cell recordings, patch electrodes (tip resistance: 3–5 MΩ) were pulled from borosilicate glass (Harvard Apparatus) and filled with internal solution containing (in mM) 138 K-gluconate, 10 HEPES, 0.0001 $CaCl_2$, 0.3 GTP-Li, and 5 ATP-Mg (pH adjusted to 7.2, osmolarity 290–305 mosM). Liquid junction potential was calculated to be $\sim$12 mV. Membrane potential (E_m) values were not corrected for the liquid junction potential since the extent to which the contents of the cells had been completely replaced with the pipette solution was unclear (Barry and Lynch 1991; Neher 1992; Onimaru et al. 1996). A micromanipulator (MPC-385, Sutter Instruments) was used to position the electrode over the cut region of the spinal cord and lower it into the tissue. IR-DIC and GFP (band pass 450–490 nm) filters were used to target EFP^+ cells located along the extend of the cut region of the spinal cord for recording. With a whole cell recording amplifier (Multiclamp 700B, Axon Instruments) in voltage-clamp mode, a 10-mV square pulse (50 Hz) was used to monitor tip resistance as the electrode was advanced toward the cell of interest. Once a gigaohm seal with a cell was formed, the command voltage was set to -60 mV and gentle suction was applied to break through the membrane to obtain a whole cell recording. Series resistance (R_S) and cell capacitance (C_m) were determined in voltage-clamp mode with the compensation features on the Multiclamp commander software (Axon Instruments). R_S was monitored throughout the course of each recording (if working in current-clamp mode, we would periodically switch into voltage clamp to monitor R_S). Initial values of R_S were typically 10–15 MΩ. Recordings where R_S exceed 30 MΩ were excluded from analysis. In some instances, a small amount of negative bias current (10–15 pA) was required to hyperpolarize the cell to prevent spontaneous firing of action potentials.

Once a stable E_m was reached, the amplifier was switched into voltage-clamp mode and we determined whether the cell possessed a persistent inward current (PIC) by applying a triangular voltage ramp from -110 to -10 mV (Tazerart et al. 2008). The speed of the voltage ramp was slow (10 s total; 12 mV/s) to avoid activation of transient sodium channels (Tazerart et al. 2008). PIC magnitude was obtained from recordings after subtraction of the leak current, which was performed with the leak subtraction tool in Clampfit (Axon Instruments). Current traces were digitally filtered (in Clampfit) before analysis and preparation of figures (low-pass Butterworth filter, 30 Hz). Membrane resistance (R_m) was calculated off-line by taking the inverse slope of the linear portion of the current-voltage (*I-V*) relationship.

In some instances, the intrinsic bursting properties of dI6 neurons were examined by reducing network drive to these cells. This was accomplished by either blocking fast glutamatergic transmission with CNQX (10 μM; Ziskind-Conhaim et al. 2008) or by inhibiting chemical synaptic transmission with a low-calcium (0.25 mM) aCSF solution (Tazerart et al. 2008). Reduction of Ca^{2+} was offset by increasing Mg^{2+} (to 3.7 mM) in order to avoid changes in osmolarity. Finally, to investigate whether neurons displayed voltage-dependent firing frequency when network input was reduced, small amounts of bias current were injected in a stepwise manner to change the holding potential of a cell between -70 mV and -40 mV.

Data analysis and statistics. In all instances in which neuronal activity was compared with fictive locomotor output, the ipsilateral ventral root in the same spinal cord segment as the recorded neuron was chosen for analysis (referred to as the local ventral root). If ENG records were not available for the local ventral root, activity in a neighboring ventral root (either the contralateral or ipsilateral L2 or L5) was normalized to represent activity in the local ventral root and was used for analysis.

To create histograms of firing frequency in order to analyze the distribution of action potentials during fictive locomotion, a single locomotor cycle (defined as the time between the onset of 2 bursts of ENG activity in a given ventral root) was divided into 10 equal bins, with *bins 1–5* representing the period of ventral root activity and *bins 6–10* representing the relatively inactive phase (i.e., the interburst interval). The frequency of action potentials occurring within each bin was calculated for 20 consecutive cycles and plotted as a histogram. The phase preference of a given neuron was determined by comparing the average spike frequency of the burst (i.e., *bins 1–5*) and interburst (i.e., *bins 6–10*) periods. In some instances, a neuron fired preferentially at the transition between the active and inactive phases. In these cases, the average spike frequency of the five consecutive bins with the highest spike frequency (e.g., *bins 3–7*) were compared with the remaining five consecutive bins (e.g., *bins 8–2*).

All means are reported ± standard deviation (SD). Unless stated otherwise, Student's *t*-tests were used to determine whether means were significantly different. Circular statistics (Zar 1974) were used to determine the coupling strength between subthreshold oscillations in E_m [i.e., locomotor drive potentials (LDPs)] and ventral root activity. LDPs in neurons occurring over the entire period of analysis (typically 5–10 min) were selected, and their phase values were calculated in reference to the onset of the local ventral root. Phase values were determined by dividing the latency between the onset of the LDP and the ventral root burst by the cycle period. This resulted in values of 0.5 when LDP and ventral roots were completely out of phase and values of 1 when they were in phase. The phase values were imported into MATLAB (The MathWorks), and a custom script was used to generate a polar plot and provide *r* values. To determine whether the sample *r* was large enough to confidently indicate a nonuniform distribution of points, Rayleigh's test ($R = nr$) was performed. The resulting value for *R* was compared with a critical values table.

Immunohistochemistry. Immunohistochemistry on frozen spinal cord sections was performed as previously described (Gross et al. 2002; Moran-Rivard et al. 2001). Serial sections of either whole embryos or early postnatal spinal cords were cut (20 μm) and incubated with primary antibodies overnight, followed by incubation with species-specific secondary antibodies conjugated with Cy2, Cy3, or Cy5 (Jackson Laboratories). After the slides were coverslipped, images were captured with a Zeiss LSM5-Pascal confocal microscope and assembled with Adobe Photoshop.

RESULTS

The Dbx1^{Cre}; Rosa26^{EFP} mouse labels dorsal V0 and dI6 interneurons. The Dbx1^{LacZ} mouse line has been shown to selectively mark all p0 progenitors and V0 interneurons (both dorsal and ventral subpopulations) with β-gal (Pierani et al. 2001; Lanuza et al. 2004). To determine whether Cre-mediated recombination was limited to the V0 neuronal population in Dbx1^{Cre} mice, this strain was mated with Rosa26^{EFP} animals and offspring that expressed EFP were subsequently crossed with the Dbx1^{LacZ} line. The Dbx1^{Cre}; Rosa26^{EFP}; Dbx1^{LacZ} mouse would thus express the reporter protein EFP in the progeny of all Cre-expressing cells and the reporter protein β-gal in all V0 interneurons. Initial inspection of the spinal cords from Dbx1^{Cre}; Rosa26^{EFP}; Dbx1^{LacZ} mice at E11.5 indicated that rather than being expressed in all β-gal$^+$ (i.e., Dbx1$^+$ derived) cells, EFP expression was shifted dorsally, beginning midway through the p0 domain and continuing slightly beyond its dorsal extent (Fig. 1*A*), into the progenitor domain that typically gives rise to the dI6 neurons (Gross et al. 2002). This led us to conclude that Cre expression does not fully recapitulate Dbx1 expression, likely because of incomplete regulatory elements included in the Dbx1 promoter transgene that was used to drive Cre expression. To definitively

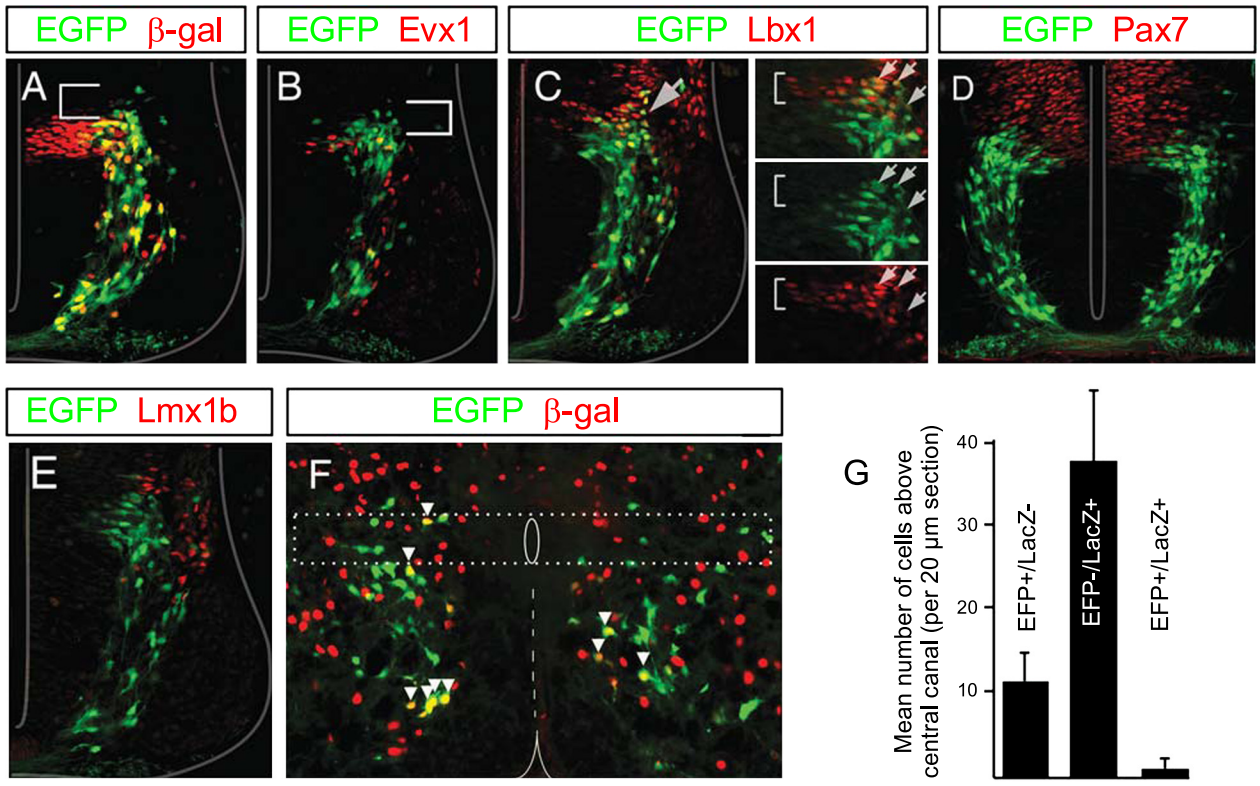

Fig. 1. Transcriptional profile of labeled neurons in Dbx1^{Cre}; Rosa26^{EFP} mouse. *A* and *B*: coronal sections of E11.5 neural tube from Dbx1^{Cre}; Rosa26^{EGFP}; Dbx1^{LacZ} mouse illustrate that enhanced green fluorescent protein (EGFP; green) is coexpressed in only a portion of β-gal$^+$ cells (i.e., V0 cells; red cells, *A*) and is not coexpressed with Evx1 (red cells, *B*), a marker of ventral V0 neurons (V0$_V$). Colocalization was confirmed by inspecting *z*-stack images compiled on a confocal microscope. A portion of EGFP$^+$ cells are situated dorsal to the V0 population (white bracketed region) *C*: cross section of an E11.5 neural tube stained with antibodies to EGFP (green) and Lbx1 (red; a marker of dorsal interneurons that is downregulated in postmitotic cells) indicates that some EGFP cells in the Dbx1^{Cre}; Rosa26^{EGFP} are dorsal spinal interneurons. Double-labeled cells are indicated by white arrows in *insets*. *D*: at E10.5 a portion of the postmitotic EGFP-marked cells (green) are derived from Pax7 cells (red), indicating that they arise from dorsal progenitors. *E*: EGFP cells (green) are located ventral to neurons expressing Lmx1b (red), a marker of the dI5 interneuronal population. *F*: coronal section from a postnatal Dbx1^{Cre}; Rosa26^{EGFP}; Dbx1^{LacZ} mouse in which dI6 cells express EGFP alone (green), V0$_D$ cells express EFP and β-gal (red and green, i.e., yellow, marked by white arrowheads), and V0$_V$ cells express β-gal only (red). Region from which electrophysiological recordings were made is outlined by dashed box. *G*: cell counts indicate that in the Dbx1^{Cre}Rosa26^{EFP}; Dbx1^{LacZ} mouse the majority of cells expressing reporter protein located above the central canal are dI6 cells (i.e., EFP only).

determine the cell population(s) in which the reporter protein was expressed, the transcriptional profile of the EFP-expressing neurons was examined. While many EFP-expressing cells coexpressed β-gal, indicating that they belong to the V0 population (Fig. 1*A*), EFP was not coexpressed with the transcription factor Evx1, a postmitotic marker of the ventral subpopulation of V0 cells ($V0_V$ cells; Moran-Rivard et al. 2001) (Fig. 1*B*), indicating that EFP is expressed in the dorsal subset of V0 cells ($V0_D$). The population of postmitotic EFP-expressing neurons located immediately dorsal to the $V0_D$ cells was found to coexpress Lbx1 while exiting the ventricular zone (Fig. 1*C*) and arise from $Pax7^+$ progenitors (Fig. 1*D*), both expressed in cells that originate in the dorsal neural tube. To determine the extent of the dorsal expression of EFP in the $Dbx1^{Cre}$; $Rosa26^{EFP}$ mouse we looked for colocalization with the transcription factor Lmx1b, which is expressed in dI5 neurons. The lack of coexpression of EFP and Lmx1b (Fig. 1*E*) led us to the conclusion that the $Dbx1^{Cre}$; $Rosa26^{EFP}$ mouse labels the $V0_D$ and dI6 cell populations with EFP.

The $Dbx1^{Cre}$; $Rosa26^{EFP}$; $Dbx1^{LacZ}$ line enabled these two populations to be identified postnatally, as dI6 cells expressed EFP alone while $V0_D$ cells expressed both EFP and β-gal (Fig. 1*F*). $V0_V$ cells could be definitively identified in these mice by the expression of β-gal alone (Fig. 1*F*). Initially, this mouse line was used for electrophysiological experiments, EFP cells were targeted, and post hoc β-gal staining was performed (see Kwan et al. 2009) to confirm that the cells investigated were dI6 (i.e., EFP^+ and $\beta\text{-gal}^-$) rather than $V0_D$ neurons. Since such a small proportion of offspring from $Dbx1^{Cre}$; $ROSA26^{EFP}$; $Dbx1^{LacZ}$ mice expressed the Cre, EFP, and LacZ alleles required to definitively differentiate between the populations (1/16 based on Mendelian genetics) we explored whether there was a more efficient manner to target dI6 cells for electrophysiological recordings. Cell counts of these three populations revealed that, on average, there were 10.9 EFP^+ cells located above the central canal per 20-μm spinal cord section in the early postnatal mouse and only 1.3 of these EFP^+ cells were $\beta\text{-gal}^+$. Thus 88 ± 8% (SD) (n = 11 spinal cords) of all EFP^+ neurons dorsal to the central canal were $\beta\text{-gal}^-$ and therefore dI6 cells (Fig. 1, *F* and *G*). Since all electrophysiological recordings in this study were taken from cells located above the central canal (region within dashed box in Fig. 1*F*) and the vast majority of EFP^+ cells in this region belonged to the dI6 population, $Dbx1^{Cre}$; $Rosa26^{EFP}$ mice were also used to target dI6 interneurons. While this significantly increased the number of offspring from which we could record, it is likely that a small proportion of the cells included in our data set belong to the $V0_D$ subpopulation.

dI6 neurons oscillate during fictive locomotion. To investigate the activity of dI6 cells during locomotor-like activity, fictive locomotion was evoked in spinal cords from neonatal $Dbx1^{Cre}$; $Rosa26^{EFP}$ or $Dbx1^{Cre}$; $Rosa26^{EFP}$; Dbx^{LacZ} mice in which the dorsal regions had been removed. Previous studies have shown that pharmacologically induced fictive locomotion is not significantly altered in this preparation (Dougherty and Kiehn 2010; Dyck and Gosgnach 2009) and that EFP^+ cells situated close to the cut surface of the spinal cord are healthy and accessible for whole cell patch-clamp recording.

In total, recordings were made from 79 EFP^+ cells after the establishment of fictive locomotion (induced by bath application of 5 μM NMDA, 10 μM 5-HT). Of these, 53% (42/79) showed oscillations in their E_m (Fig. 2, *A* and *B*), while the remaining 47% (36/79) spiked tonically or were silent during fictive locomotion. As we were interested in examining the role of the dI6 neurons during locomotor activity, we restricted our study to those cells that were rhythmically active. To determine whether activity in the oscillatory cells was directly related to fictive locomotor outputs, the firing frequency of each cell was calculated during the normalized ventral root burst cycle and plotted as a histogram (Fig. 2, *C* and *D*) (Butt and Kiehn 2003). In 88% (37/42) of the cells, the firing pattern showed a significant ($P < 0.05$, t-test) phase preference, with 40% (17/42) firing preferentially during the active phase of the ipsilateral ventral root in which the interneuron was located (i.e., the local ventral root), 33% (14/42) firing in the inactive phase of the local ventral root, and 14% (6/42) firing at the transition between the burst and interburst periods. Even in those cases in which the phase preference of the dI6 neuron was statistically significant, the majority of cells (34/42) did fire >15% of action potentials in their nonpreferred phase (Fig. 2, *A* and *C*). These cells are referred to as loosely coupled (LC) dI6 neurons. In the remaining oscillatory EFP^+ neurons (8/42), oscillations were tightly coupled to ventral root output and <15% of action potentials were observed in their nonpreferred phase (Fig. 2, *B* and *D*). These neurons are referred to as tightly coupled (TC) dI6 neurons.

TC and LC dI6 neurons are electrophysiologically distinct. Initial assessment of intrinsic membrane properties recorded from dI6 interneurons that were rhythmically active during fictive locomotion (see Table 1) revealed that while LC and TC cells did not differ significantly with respect to mean resting E_m ($P > 0.1$ Welsh's t-test for unequal sample sizes), LC cells (mean R_m = 1,041 ± 541 MΩ) were significantly smaller ($P < 0.05$, Welsh's t-test for unequal sample sizes) than TC interneurons (mean R_m = 546 ± 171 MΩ). Values for R_m and resting E_m were found to be similar to those recorded from interneurons in a similar location (Quinlan and Kiehn 2007; Tazerart et al. 2008). To characterize the dorsally located dI6 interneurons and examine their potential function during fictive locomotion we investigated whether rhythmic oscillations in either subclass were due to intrinsic membrane properties. To this end, fictive locomotion was evoked by application of 5-HT and NMDA and whole cell recordings were made from EFP cells. Upon confirmation that a cell was rhythmically active during fictive locomotion and classification of the cell as either a TC or a LC interneuron, network inputs were inhibited (by reducing the Ca^{2+} concentration of the r-aCSF solution) or fast excitatory synaptic transmission was abolished (by bath application of 10 μM CNQX). Preparations were considered to be sufficiently isolated once rhythmic ventral root activity ceased.

Although the amplitude and duration of the oscillatory activity in LC dI6 neurons was altered, rhythmic activity in these cells persisted when isolated (n = 10/10 CNQX, Fig. 3*A*, *i* and *ii*; n = 8/8 low Ca^{2+}, Fig. 3*B*, *i* and *ii*), suggesting that these cells are conditional oscillators. Oscillations in TC dI6 neurons, on the other hand, were clearly abolished when isolated from fast excitatory inputs (n = 4/4 CNQX, Fig. 3*C*, *i* and *ii*), demonstrating that these cells have no intrinsic oscillatory capability. These results provide evidence that LC and TC dI6 neurons are electrophysiologically distinct and raise the possibility that LC neurons may be involved in driving rhythmic activity in the locomotor CPG.

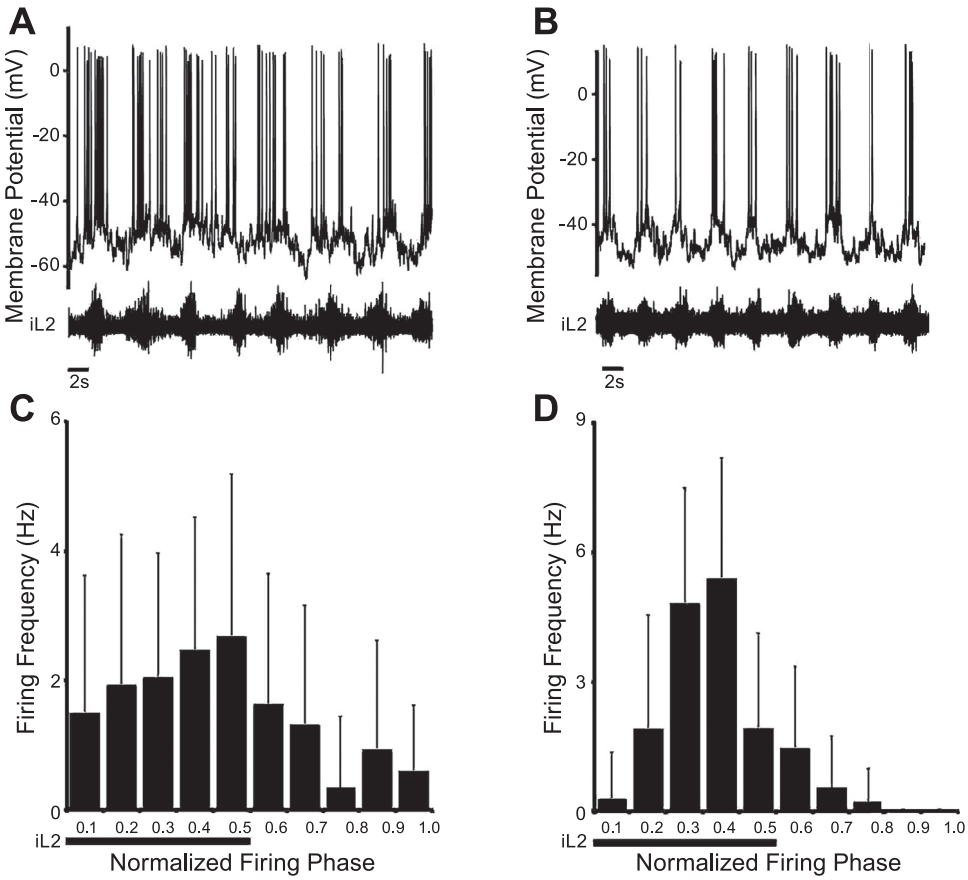

Fig. 2. Firing patterns of oscillatory dI6 neurons during fictive locomotion. *A* and *B*: typical activity pattern of loosely coupled (LC; *A*) and tightly coupled (TC; *B*) dI6 neurons during fictive locomotion induced by bath application of 5-hydroxytryptamine (5-HT) and *N*-methyl-D-aspartate (NMDA). *C* and *D*: instantaneous firing frequency within 1 normalized step cycle for LC and TC dI6 neurons shown in *A* and *B*. *Bins 1–5* represent the period of local ventral root activity (iL2), and *bins 6–10* represent the inactive phase (i.e., the interburst interval).

In light of their ability to oscillate while isolated from network inputs, we were interested to determine whether the LC cells possessed other signature intrinsic properties of rhythm-generating neurons. Multiple studies have suggested that a riluzole-sensitive PIC is required for locomotor rhythm generation (Rybak et al. 2006; Sherwood et al. 2011; Tazerart et al. 2007, 2008; Zhong et al. 2007). To determine whether LC interneurons possess this current, the *I-V* relationship of these cells was analyzed by applying a slow voltage ramp (12 mV/s) to a cell while it was held in voltage clamp. In LC neurons, a PIC could be seen ($n = 34/34$; Fig. 4*A*) as a region of negative slope conductance during the depolarization phase of the ramp (Lee and Heckman 1999; Li and Bennett 2003). The PIC had a mean onset at −38 mV (−50 mV if 12-mV liquid junction potential is taken into account) and an average leak-subtracted magnitude of 29.81 ± 10.88 pA (Table 1). We propose that a persistent sodium current is responsible since a low concentration of riluzole (5 μM) successfully abolished the region of negative slope conductance in all cases in which it was applied (3/3; Fig. 4*A*). In contrast, PICs were not observed in any of the eight TC dI6 neurons in response to the same voltage ramp (Fig. 4*B*).

In addition to nonlinear membrane properties, cells involved in locomotor rhythm generation have been shown to display intrinsic voltage sensitivity when isolated from excitatory synaptic transmission, such that the frequency of oscillations depends on the holding potential of the cell (Hochman et al. 1994; Kiehn et al. 1996; Tazerart et al. 2008; Wilson et al. 2005). This property is thought to be essential for driving the rhythm at various speeds (Brownstone and Wilson 2008). To determine whether LC dI6 interneurons are able to modulate oscillation frequency, CNQX or low-Ca^{2+} solution was added to the preparation, cells were held in current-clamp mode, and current steps were applied to depolarize (to −40 mV) or hyperpolarize (to −70 mV) the cell. Frequency of oscillations (evoked by 5 μM NMDA, 10 μM 5-HT) at each holding potential was recorded. As expected, oscillations in the majority of LC dI6 neurons (10/18) fired in a voltage-dependent manner, with the frequency of oscillations increasing when the cell was depolarized and decreasing when hyperpolarized (Fig. 4, *C* and *D*).

TC dI6 interneurons receive rhythmic inputs from the locomotor CPG. Given the clear rhythmic oscillations observed in the TC cells and their inability to oscillate intrinsically and lack

Table 1. *Membrane properties of TC and LC interneurons*

Cell Type	*n*	E_m, mV	Mean R_m, MΩ	Mean PIC Magnitude, pA	Mean PIC Onset, mV
TC	8	47.3 ± 5.15	546 ± 171	—	—
LC	34	50.3 ± 5.3	1,041 ± 541	29.81 ± 10.88	38.73 ± 5.99

Data are means ± SD for *n* neurons. TC, tightly coupled; LC, loosely coupled; E_m, membrane potential; R_m, membrane resistance; PIC, persistent inward current.

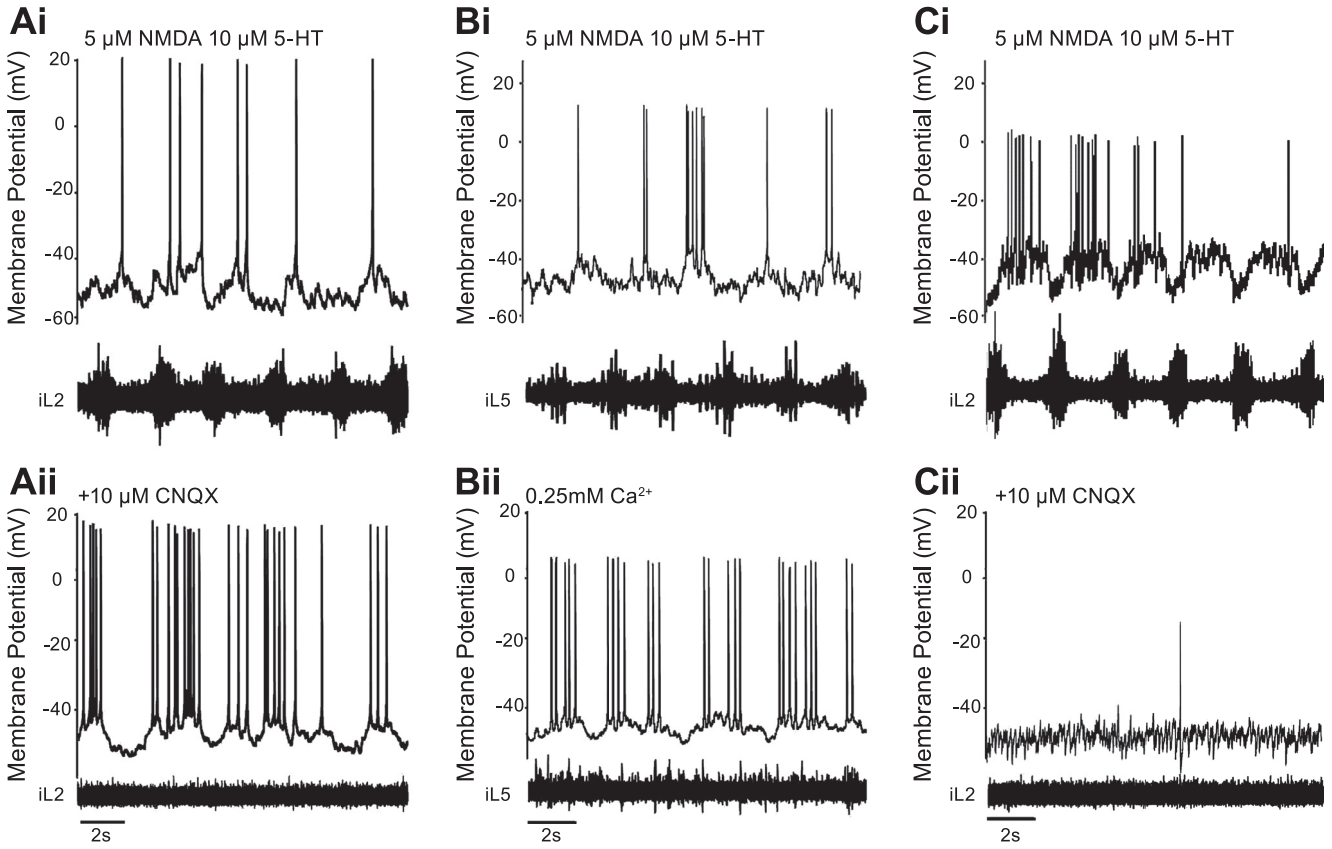

Fig. 3. LC, but not TC, dI6 neurons oscillate intrinsically. *A*: oscillations in a LC dI6 neuron during fictive locomotion evoked by bath application of 5-HT and NMDA (*i*) persist after blockade of all fast non-NMDA glutamatergic synaptic transmission with 10 μM CNQX (*ii*). *B*: similar effect is seen in another LC dI6 cell (*i*) after application of a low-calcium (0.25 mM) artificial cerebrospinal fluid (aCSF) solution (*ii*). Note that, in both cases, fictive locomotor activity is abolished in the ventral root after the reduction of network input (*Aii*, *Bii*). *C*: when 10 μM CNQX is applied to an oscillatory TC dI6 cell (*i*), rhythmicity is abolished in both the neuron and the ventral root (*ii*), indicating that these cells are not oscillatory.

of a PIC, we hypothesized that rather than being involved in generating the locomotor rhythm, these cells receive outputs from the locomotor CPG and are involved in coordinating motoneuron activity during locomotion. To investigate this, we first compared the oscillation frequency of the TC dI6 cells to the frequency of ENG bursts recorded from the local ventral root and found that these values were almost identical in all cases [mean TC dI6 frequency = 0.350 ± 0.035 Hz (SD);

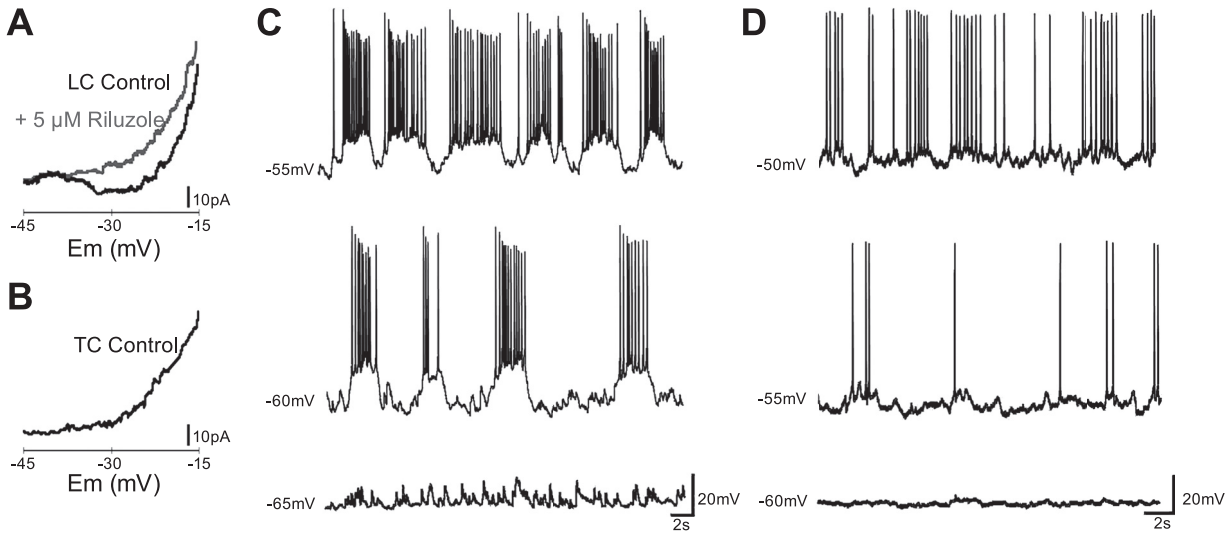

Fig. 4. LC, but not TC, dI6 neurons possess nonlinear membrane properties. *A*: a persistent inward current (PIC, indicated by region of negative slope conductance in the current-voltage plot) is evoked in an LC dI6 neuron in response to a voltage ramp (black trace). Bath application of riluzole (5 μM) inhibits the PIC in the same neuron (gray trace). E_m, membrane potential. *B*: no PIC is evident in a TC dI6 neuron in response to the same triangular voltage ramp. *C* and *D*: after bath application of 10 μM CNQX (*C*) and low-calcium (0.25 mM) aCSF solution (*D*), oscillation frequency in 2 LC dI6 neurons increases in response to depolarization of the E_m at which the cell is held.

mean ventral root frequency = 0.357 ± 0.035 Hz (SD); $n = 8$]. The strength of this coupling was not altered after current injection (Fig. 5).

The strength of coupling between LDPs recorded from TC dI6 neurons and ENG activity during fictive locomotion was also analyzed by circular statistics, which allowed the relationship to be represented as a data point on a circular plot (Fig. 6*B*). Each point in Fig. 6*B* represents the phase value of the delay between the onset of the LDP and the onset of the ENG burst in the local ventral root for the trial illustrated in Fig. 6*A*. Data points at 0.0 represent synchronous onset of LDP and ENG burst, and points at 0.5 represent LDP and ENG bursts that are perfectly out of phase. The *R* value (which determines coupling strength of the neuron with ENG activity) for this cell was 0.89, indicating that it was tightly coupled to ventral root activity. This was representative of the entire TC population, in which the mean *R* value was 0.893 ± 0.06 (SD) ($n = 8$). Data points in Fig. 6*C* represent the mean vector point for each individual TC dI6 cell.

Finally, if TC dI6 interneurons are involved in coordinating motoneuron bursting during locomotor activity, they would comprise part of the "pattern-forming" layer of the recently proposed two-layer model of the locomotor CPG (Rybak et al. 2006). To determine whether this was the case, their behavior was analyzed during spontaneous omissions of activity (i.e., deletions) that occur during fictive locomotion. As components of the pattern-forming layer they would be expected to either decrease their output (if related to the agonist motoneuron species in which deletion occurs) or increase their output (if related to the antagonist) during a nonresetting deletion. Nonresetting deletions were observed in four experiments. In all cases the TC neuron was located in the same segment as the ventral root in which the deletion occurred, on the contralateral side of the spinal cord. All four TC cells had a activity pattern similar to that illustrated in Fig. 6*D*, in which a deletion in the left L2 ventral root is accompanied by a reduction of activity (and the absence of action potentials) in the TC neuron located in the contralateral L2 segment. Since deletions have often been shown to occur in antagonist motoneuron pools bilaterally (Talpalar and Kiehn 2010), this would suggest that the TC neurons comprise part of the pattern-forming layer and coordinate motoneuron activity during locomotion.

DISCUSSION

Although it has previously been postulated that dI6 cells are a population of commissurally projecting, inhibitory interneurons that are involved in locomotor behavior (Goulding 2009; Lanuza et al. 2004; Rabe et al. 2009), the lack of a unique

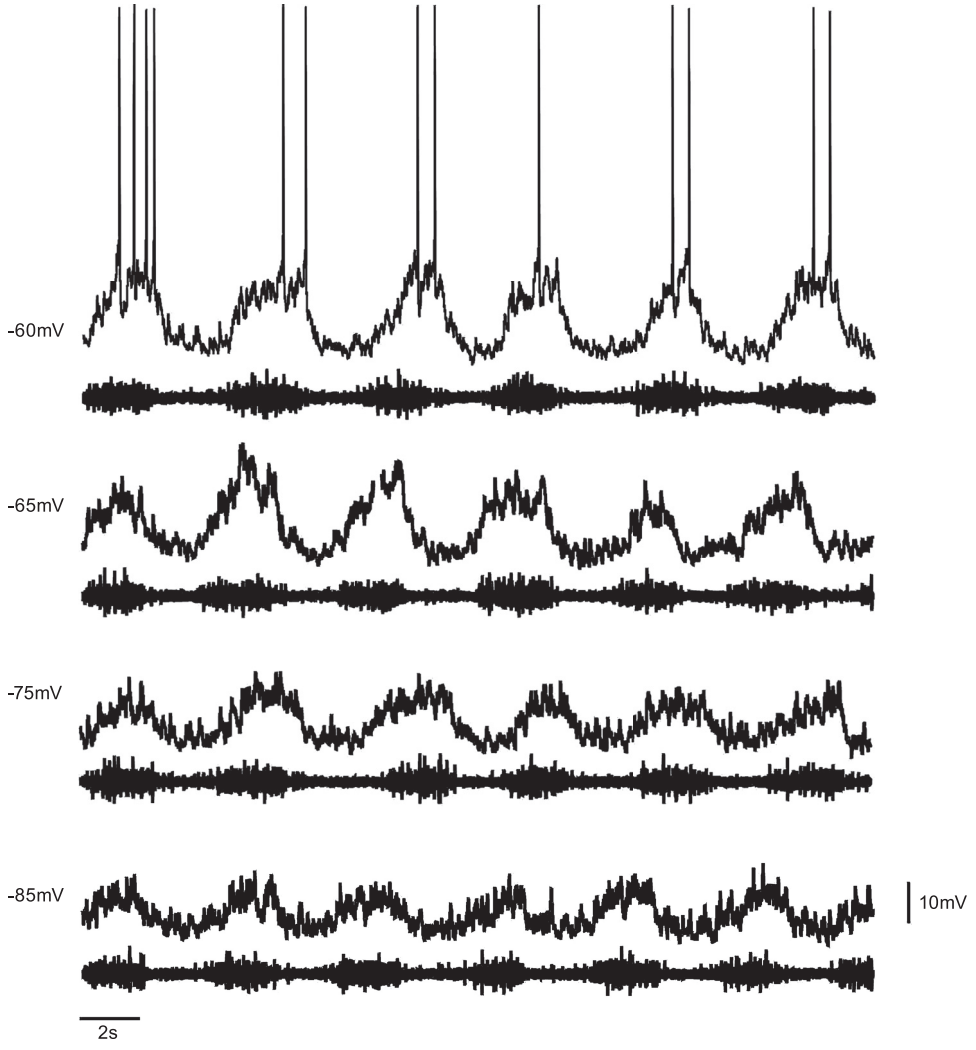

Fig. 5. Oscillations in TC dI6 neurons are voltage insensitive. Current-clamp recording from a TC dI6 neuron during fictive locomotion in which the membrane potential is varied through intracellular current injection. At all holding potentials the cell bursts together with the local ventral root.

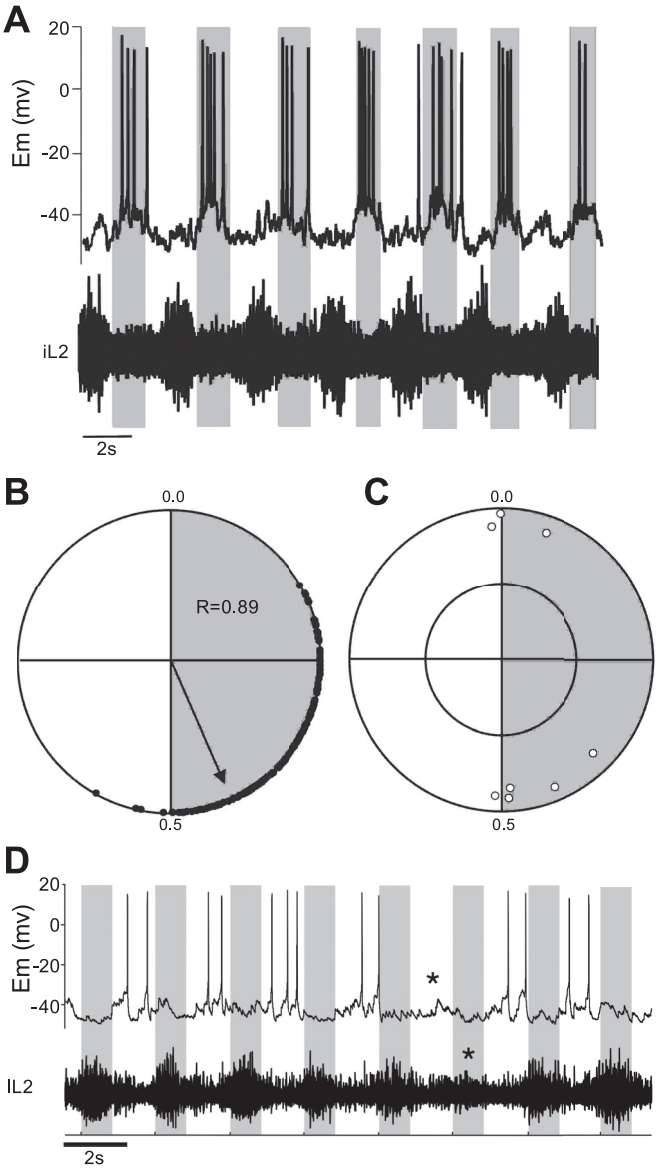

Fig. 6. TC dI6 neurons receive highly rhythmic drive potentials. *A*: current-clamp recording of a oscillatory TC dI6 interneuron that bursts out of phase with the local ventral root (iL2). *B*: polar plot for neuron shown in *A* compares onset of ventral root ENG activity and locomotor drive potential (LDP) onset and demonstrates that they are out of phase (i.e., points clustered around 0.5). *C*: group polar plot for all TC dI6 neurons (white circles) demonstrates that they burst consistently in, or out of, phase with the local ventral root. *D*: example of a nonresetting deletion seen in a TC neuron (located in the right L2 segment) as well as ENG activity pattern recorded from the contralateral L2 ventral root. During "normal" fictive locomotion the neuron bursts out of phase with activity in the ventral root. When a nonresetting deletion occurs in the ventral root (shaded box with *), it is accompanied by a reduction of activity and lack of action potentials in the preceding active phase of the contralateral TC cell (unshaded region with *). Following the deletion rhythm in the TC cell and the ventral root maintains the timing of activity that preceded the deletion.

molecular marker for these cells has not allowed these hypotheses to be tested. Here we used a transgenic mouse line that labels the $Dbx1^+$ $V0_D$ cells as well as dI6 interneurons, a population that develops immediately dorsal to the $V0_D$ cells from $Dbx1^-$, $Lbx1^+$, $Pax7^+$ progenitors. While unexpected, labeling of dI6 cells in this mouse enabled visually guided recordings to be made from this population, and the present work is the first to describe their intrinsic electrophysiological properties. To provide insight into their role during locomotor activity, we utilized a preparation in which a notch is removed from the dorsal aspect of the spinal cord, allowing dI6 interneurons located dorsal to the central canal to be investigated during fictive locomotion. While a definitive description of the function of dI6 neurons in the locomotor CPG must await an effective approach of selectively silencing or ablating this population, our findings demonstrate that many of these cells are rhythmically active during locomotor activity, and that the majority of these possess intrinsic oscillatory properties. These data raise the possibility that a significant proportion of dI6 neurons may be involved in locomotor rhythm generation.

LC dI6 interneurons are able to oscillate intrinsically. By far the most common firing pattern observed among rhythmically active dI6 interneurons (34/42) was a loose coupling to fictive locomotor activity recorded from the ventral roots. These cells are referred to as "loosely coupled" since action potentials were often seen in their nonpreferred phase during fictive locomotion. Several characteristics of this subclass of dI6 interneurons lead us to suggest that they may be involved in locomotor rhythm generation. First, these cells are located in laminae VII/VIII of the thoraco-lumbar spinal cord, a region that has been shown to receive monosynaptic contacts from brain stem centers responsible for generating rhythmic, locomotor activity in the spinal cord (Matsuyama et al. 2004) and is essential for the induction of fictive locomotion in the isolated preparation (Antri et al. 2011; Kjaerulff and Kiehn 1996). Second, the LC dI6 interneurons possess many intrinsic membrane properties that have been suggested to be essential for the rhythm-generating neurons of the locomotor CPG (Brownstone and Wilson 2008). These cells are able to oscillate at multiple frequencies when isolated from excitatory input (Fig. 3, *A* and *B*, Fig. 4, *C* and *D*) and exhibit a riluzole-sensitive PIC (Fig. 4*A*). While the presence of a PIC does not, in and of itself, demonstrate a role in rhythm generation (PICs are present in motoneurons that are not part of the rhythm-generating network), recent work indicates a direct link between locomotor rhythm generation and the presence of persistent sodium currents in spinal interneurons (Tazerart et al. 2008; Zhong et al. 2007). Furthermore, recent computational models of the locomotor CPG suggest that neurons that generate rhythmic activity rely on a sodium-dependent PIC for intrinsic oscillations (Rybak et al. 2006; Sherwood et al. 2011).

Rhythmic bursting in TC dI6 interneurons is phase locked to motoneuron activity. In contrast to the population of dI6 interneurons that were loosely coupled to fictive locomotion, we recorded from relatively few (8/42) interneurons that were tightly coupled to ENG activity. The phase-locked nature of oscillations in TC dI6 interneurons and the ventral roots during normal fictive locomotor activity (Fig. 5), as well as during irregularities in the fictive locomotor pattern (Fig. 6*D*), suggests that this subclass of cells may be involved in the regulation of motoneuron activity. Although we did not have a mechanism of quantitatively measuring the medial-lateral location of these cells in our preparation, TC cells tended to be located more laterally than the LC dI6 interneurons (J. Dyck, unpublished observation), in a region of the lumbar spinal cord that has been shown to contain many interneurons that make direct contact onto, and regulate the activity of, ipsilateral motoneurons (Coulon et al. 2011; Stepien et al. 2010). Further support for the hypothesis that TC cells regulate motoneuron

firing comes from the fact that dI6 cells are closely related to the V0 population, which have been shown to make monosynaptic connections onto motoneurons and regulate their activity during fictive locomotion (Lanuza et al. 2004). Both the dorsal population of V0 cells and the dI6 population develop from similar progenitors (Gross et al. 2002; Muller et al. 2002; Pierani et al. 2001) and migrate along a similar ventromedial pathway during embryogenesis (Gross et al. 2002; Moran-Rivard et al. 2001; Pierani et al. 2001). In light of these similarities, and multiple predictions that dI6 and V0 interneurons play an analogous role during locomotor activity (Goulding 2009; Rabe et al. 2009), we were surprised that so few dI6 cells from which we recorded fit into the TC category.

It is important not to lose sight of two caveats with this study. First, based on cell counts (Fig. 1*G*) it is likely that a small proportion (12%) of the EFP^{+} cells from which we recorded in the $Dbx1^{Cre}$; $Rosa26^{EFP}$ mice were $V0_D$ cells rather than dI6 cells. Since previous work has shown that the $V0_D$ population is involved in coordination of left-right alternation (Lanuza et al. 2004), it is likely that some cells that were categorized as TC dI6 cells were, in fact, $V0_D$ cells and the proportion of dI6 cells located close to the central canal that are involved in motoneuron coordination is slightly overestimated. Second, all whole cell recordings in this study were made from EFP^{+} neurons located above the ventral extent of the central canal (Fig. 1*F*). We were therefore unable to determine whether more ventrally located dI6 neurons fit into one of the categories described here, or whether they represent a distinct subpopulation of dI6 neurons. Given the fact that the majority of interneurons that have previously been shown to project to motoneurons are located ventral to the central canal (Butt and Kiehn 2003; Hinckley et al. 2005; Lanuza et al. 2004; Quinlan and Kiehn 2007; Stepien et al. 2010; Zhang et al. 2008) and the paucity of TC dI6 interneurons from which we recorded, we postulate that the majority of ventrally located dI6 neurons fit into the TC category and are involved in coordinating motoneuron output.

Network implications. To date, no single genetically defined interneuronal population has been shown to be necessary and sufficient for the generation of rhythmic activity in the locomotor CPG. In fact, locomotor-like activity persists after the deletion and/or silencing of each of the V0 (Lanuza et al. 2004), V1 (Gosgnach et al. 2006), V2a (Crone et al. 2008), and V3 (Zhang et al. 2008) interneuronal populations, and Hb9 interneurons have a firing pattern inconsistent with locomotor rhythm generation (Kwan et al. 2009). In light of the studies that have demonstrated that the region encompassing the central canal of the thoraco-lumbar spinal cord is essential for generation of locomotor activity (Antri et al. 2011; Kjaerulff and Kiehn 1996), and the fact that the dI6 interneurons together with the aforementioned V0, V2a, V3, and Hb9 populations make up the majority of cells located in this area postnatally, we predict that the generation of activity in the locomotor CPG must be due to either the dI6 interneurons alone or a shared role among several populations located in this area.

Because of the irregular rhythm seen in the LC dI6 cells when isolated from network inputs (Fig. 3, *A* and *B*), we believe that the latter of these hypotheses is more plausible and the LC dI6 cells work together with other interneurons, located in close proximity, to generate the locomotor rhythm. Subsets of other genetically defined interneuronal populations close to the central canal (i.e., Hb9 and V2a) have been shown to possess many features of rhythmogenic cells (Dougherty and Kiehn 2010; Wilson et al. 2005); however, each population has been demonstrated to be incapable of independently generating the locomotor rhythm (Crone et al. 2008; Kwan et al. 2009). Given their intrinsic properties and anatomical location, we speculate that subsets of each of these populations, together with the LC dI6 interneurons, constitute the rhythm-generating core of the locomotor CPG that drives activity in a network of so-called "pattern-forming" cells (Lafreniere-Roula and McCrea 2005) that project directly onto motoneurons (Fig. 7). This general organizational principle is supported by the observation that V2a interneurons (part of proposed rhythm-generating core) make monosynaptic contacts onto commissural V0 interneurons (Crone et al. 2008), a subset of which are known to project to, and inhibit, contralateral motoneurons (Lanuza et al. 2004) and thus constitute part of the pattern-forming layer. Recent tracing studies indicate that the Hb9 interneurons (Hinckley et al. 2005) as well as subsets of the dI3 and V2a populations also make monosynaptic contact onto ipsilateral motoneurons (Stepien et al. 2010) and suggest that these cells, along with the TC dI6 interneurons, may comprise the pattern-forming layer.

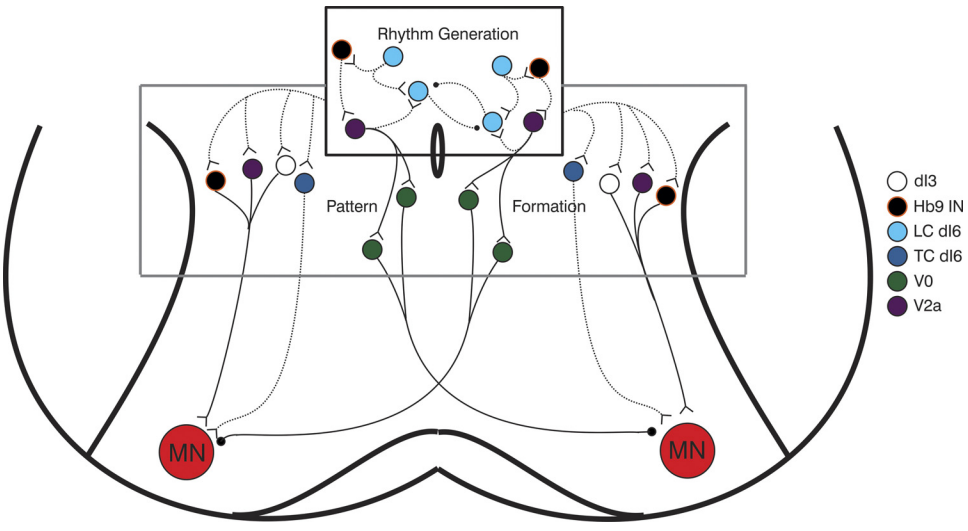

Fig. 7. Postulated organization of locomotor central pattern generator (CPG). V2a, Hb9, and LC dI6 interneurons are postulated to comprise the rhythm-generating core of the locomotor CPG and receive descending input from brain stem centers known to initiate rhythmic locomotor activity in the spinal cord. We propose that these cells provide input onto the pattern-forming layer that includes dI3, V2a, V0, Hb9 and TC dI6 cells. Members of the pattern-forming layer make direct connections onto motoneurons (MN). Documented synaptic connectivity indicated by solid lines, proposed synaptic connectivity by dashed lines. Inhibitory terminal indicated by black ball, excitatory terminal by open triangle.

In this article we incorporate two electrophysiologically distinct populations of dI6 interneurons into a recently devised two-layer model of the mammalian locomotor CPG (Rybak et al. 2006). It bears mentioning that this is only one of a number of proposed models (Grillner 1981; Kiehn et al. 2010; Kiehn 2011; Perret and Cabelguen 1980; Talpalar et al. 2011), and that several of these incorporate specific populations of genetically defined interneurons. Despite this work, a substantial amount of neuronal circuitry that has been shown to be essential for appropriate locomotor activity remains unidentified. Future studies investigating the locomotor pattern in the absence of the dI6 cells, as well as those that identify their neurotransmitter phenotype and axonal projection pattern, will enable the function of these cells during locomotion to be definitively determined and the validity of the model proposed here to be tested.

ACKNOWLEDGMENTS

We thank Dr. Martyn Goulding (Salk Institute, La Jolla, CA) for providing us with the $Dbx1^{Cre}$ and $Dbx1^{LacZ}$ mouse strains. Kenneth Wong provided technical assistance.

GRANTS

This research was supported by grants from the Canadian Institutes for Health Research (CIHR), Alberta Innovates—Health Solutions (AIHS), and the Canadian Foundation for Innovation to S. Gosgnach and the Agencia Nacional de Promoción Científica y Tecnológica PICT2006 and Fogarty International Center, National Institutes of Health to G. M. Lanuza. J. Dyck is supported by studentships from the CIHR and AIHS. G. M. Lanuza is an investigator of the Argentine National Research Council (CONICET).

DISCLOSURES

No conflicts of interest, financial or otherwise, are declared by the author(s).

AUTHOR CONTRIBUTIONS

Author contributions: J.D., G.M.L., and S.G. performed experiments; J.D., G.M.L., and S.G. analyzed data; J.D., G.M.L., and S.G. interpreted results of experiments; J.D., G.M.L., and S.G. prepared figures; J.D., G.M.L., and S.G. edited and revised manuscript; J.D., G.M.L., and S.G. approved final version of manuscript; S.G. conception and design of research; S.G. drafted manuscript.

REFERENCES

Antri M, Mellen N, Cazalets JR. Functional organization of locomotor interneurons in the ventral lumbar spinal cord of the newborn rat. *PLoS One* 6: e20529, 2011.

Barry PH, Lynch JW. Liquid junction potentials and small cell effects in patch-clamp analysis. *J Membr Biol* 212: 101–117, 1991.

Brownstone R, Wilson J. Strategies for delineating spinal locomotor rhythm-generating networks and the possible role of Hb9 interneurones in rhythmogenesis. *Brain Res Rev* 57: 64–76, 2008.

Butt SJ, Kiehn O. Functional identification of interneurons responsible for left-right coordination of hindlimbs in mammals. *Neuron* 38: 953–963, 2003.

Chung JH, Whiteley M, Felsenfeld G. A 5′ element of the chicken beta-globin domain serves as an insulator in human erythroid cells and protects against position effect in *Drosophila*. *Cell* 74: 505–514, 1993.

Coulon P, Bras H, Vinay L. Characterization of last-order premotor interneurons by transneuronal tracing with rabies virus in the neonatal mouse spinal cord. *J Comp Neurol* 519: 3470–3487, 2011.

Cowley KC, Schmidt BJ. Regional distribution of the locomotor pattern-generating network in the neonatal rat spinal cord. *J Neurophysiol* 77: 247–259, 1997.

Crone SA, Quinlan KA, Zagoraiou L, Droho S, Restrepo CE, Lundfald L, Endo T, Setlak J, Jessell TM, Kiehn O, Sharma K. Genetic ablation of V2a ipsilateral interneurons disrupts left-right locomotor coordination in mammalian spinal cord. *Neuron* 60: 70–83, 2008.

Crone SA, Zhong G, Harris-Warrick R, Sharma K. In mice lacking V2a interneurons, gait depends on speed of locomotion. *J Neurosci* 29: 7098–7109, 2009.

Dougherty K, Kiehn O. Firing and cellular properties of V2a interneurons in the rodent spinal cord. *J Neurosci* 30: 24–37, 2010.

Dyck J, Gosgnach S. Whole cell recordings from visualized neurons in the inner laminae of the functionally intact spinal cord. *J Neurophysiol* 102: 590–597, 2009.

Gosgnach S, Lanuza GM, Butt SJ, Saueressig H, Zhang Y, Velasquez T, Riethmacher D, Callaway EM, Kiehn O, Goulding M. V1 spinal neurons regulate the speed of vertebrate locomotor outputs. *Nature* 440: 215–219, 2006.

Goulding M. Circuits controlling vertebrate locomotion: moving in a new direction. *Nat Rev Neurosci* 10: 507–518, 2009.

Grillner S. Control of locomotion in bipeds, tetrapods, and fish. In: *Handbook of Physiology. The Nervous System. Motor Control*. Bethesda, MD: Am Physiol Soc, 1981, sect. 1, vol. II, p. 1179–1236.

Gross MK, Dottori M, Goulding M. Lbx1 specifies somatosensory association interneurons in the dorsal spinal cord. *Neuron* 34: 535–549, 2002.

Hinckley CA, Hartley R, Wu L, Todd A, Ziskind-Conhaim L. Locomotor-like rhythms in a genetically distinct cluster of interneurons in the mammalian spinal cord. *J Neurophysiol* 93: 1439–1449, 2005.

Hochman S, Jordan LM, MacDonald JF. *N*-methyl-D-aspartate receptor-mediated voltage oscillations in neurons surrounding the central canal in slices of rat spinal cord. *J Neurophysiol* 72: 565–577, 1994.

Kiehn O. Locomotor circuits in the mammalian spinal cord. *Annu Rev Neurosci* 29: 279–306, 2006.

Kiehn O. Development and functional organization of spinal locomotor circuits. *Curr Opin Neurobiol* 21: 100–109, 2011.

Kiehn O, Johnson BR, Raastad M. Plateau properties in mammalian spinal interneurons during transmitter-induced locomotor activity. *Neuroscience* 75: 263–273, 1996.

Kiehn O, Dougherty KJ, Hägglund M, Borgius L, Talpalar A, Restrepo CE. Probing spinal circuits controlling walking in mammals. *Biochem Biophys Res Commun* 396: 11–18, 2010.

Kjaerulff O, Kiehn O. Distribution of networks generating and coordinating locomotor activity in the neonatal rat spinal cord in vitro: a lesion study. *J Neurosci* 16: 5777–5794, 1996.

Kwan AC, Dietz SB, Webb WW, Harris-Warrick RM. Activity of Hb9 interneurons during fictive locomotion in mouse spinal cord. *J Neurosci* 29: 11601–11613, 2009.

Lafreniere-Roula M, McCrea DA. Deletions of rhythmic motoneuron activity during fictive locomotion and scratch provide clues to the organization of the mammalian central pattern generator. *J Neurophysiol* 94: 1120–1132, 2005.

Lanuza GM, Gosgnach S, Pierani A, Jessell TM, Goulding M. Genetic identification of spinal interneurons that coordinate left-right locomotor activity necessary for walking movements. *Neuron* 42: 375–386, 2004.

Lee RH, Heckman CJ. Enhancement of bistability in spinal motoneurons in vivo by the noradrenergic alpha-1 agonist methoxamine. *J Neurophysiol* 81: 2164–2174, 1999.

Li Y, Bennett DJ. Persistent sodium and calcium currents cause plateau potentials in motoneurons of chronic spinal rats. *J Neurophysiol* 90: 857–869, 2003.

Lu S, Shashikant CS, Ruddle FH. Separate cis-acting elements determine the expression of mouse Dbx gene in multiple spatial domains of the central nervous system. *Mech Dev* 58: 193–202, 1996.

Lundfald L, Restrepo CE, Butt SJ, Peng CY, Droho S, Endo T, Zeilhofer HU, Sharma K, Kiehn O. Phenotype of V2-derived interneurons and their relationship to the axon guidance molecule EphA4 in the developing mouse spinal cord. *Eur J Neurosci* 26: 2989–3002, 2007.

Matsuyama K, Nakajima K, Mori F, Aoki M, Mori S. Lumbar commissural interneurons with reticulospinal inputs in the cat: morphology and discharge patterns during fictive locomotion. *J Comp Neurol* 474: 546–561, 2004.

Moran-Rivard L, Kagawa T, Saueressig H, Gross MK, Burrill J, Goulding M. Evx1 is a postmitotic determinant of V0 interneuron identity in the spinal cord. *Neuron* 29: 385–399, 2001.

Muller T, Brohmann H, Pierani A, Heppenstall AP, Lewin GR, Jessell TM, Birchmeier C. The homeodomain factor Lbx1 distinguishes two major programs of neuronal differentiation in the dorsal spinal cord. *Neuron* 34: 551–562, 2002.

Neher E. Correction for liquid junction potentials in patch clamp experiments. *Methods Enzymol* 207: 123–131, 1992.

Onimaru H, Ballanyi K, Richter DW. Calcium-dependent responses in neurons of the isolated respiratory network of newborn rats. *J Physiol* 491: 677–695, 1996.

Perret C, Cabelguen JM. Main characteristics of the hindlimb locomotor cycle in the decorticate cat with special reference to bifunctional muscles. *Brain Res* 187: 333–352, 1980.

Perret C, Cabelguen JM, Orsal D. Analysis of the pattern of activity in "knee flexor" motoneurons during locomotion in the cat. In: *Stance and Motion: Facts and Concepts*, edited by Gurfinkle VS, Ioffe ME, Massion J, Roll JP. New York: Plenum, 1988, p. 133–141.

Pierani A, Moran-Rivard L, Sunshine MJ, Littman DR, Goulding M, Jessell TM. Control of interneuron fate in the developing spinal cord by the progenitor homeodomain protein Dbx1. *Neuron* 29: 367–384, 2001.

Quinlan KA, Kiehn O. Segmental, synaptic actions of commissural interneurons in the mouse spinal cord. *J Neurosci* 27: 6521–6530, 2007.

Rabe N, Gezelius H, Vallstedt A, Memic F, Kullander K. Netrin-1-dependent spinal interneuron subtypes are required for the formation of left-right alternating locomotor circuitry. *J Neurosci* 29: 15642–15649, 2009.

Rybak I, Shevtsova N, Lafreniere-Roula M, McCrea D. Modeling spinal circuitry involved in locomotor pattern generation: insights from deletions during fictive locomotion. *J Physiol* 577: 617–639, 2006.

Sherwood WE, Harris-Warrick R, Guckenheimer J. Synaptic patterning of left-right alternation in a computational model of the rodent hindlimb central pattern generator. *J Comput Neurosci* 30: 323–360, 2011.

Stepien A, Tripodi M, Arber S. Monosynaptic rabies virus reveals premotor network organization and synaptic specificity of cholinergic partition cells. *Neuron* 68: 456–472, 2010.

Talpalar AE, Kiehn O. Glutamatergic mechanisms for speed control and network operation in the rodent locomotor CPG. *Front Neural Circuits* 4: 19, 2010.

Talpalar AE, Endo T, Löw P, Borgius L, Hägglund M, Dougherty KJ, Ryge J, Hnasko TS, Kiehn O. Identification of minimal neuronal networks involved in flexor-extensor alternation in the mammalian spinal cord. *Neuron* 71: 1071–1084, 2011.

Tazerart S, Viemari JC, Darbon P, Vinay L, Brocard F. Contribution of persistent sodium current to locomotor pattern generation in neonatal rats. *J Neurophysiol* 98: 613–628, 2007.

Tazerart S, Vinay L, Brocard F. The persistent sodium current generates pacemaker activities in the central pattern generator for locomotion and regulates the locomotor rhythm. *J Neurosci* 28: 8577–8589, 2008.

Wilson JM, Hartley R, Maxwell DJ, Todd AJ, Lieberam I, Kaltschmidt JA, Yoshida Y, Jessell TM, Brownstone RM. Conditional rhythmicity of ventral spinal interneurons defined by expression of the Hb9 homeodomain protein. *J Neurosci* 25: 5710–5719, 2005.

Zar JH. Circular distribution. In: *Biostatistical Analysis*. Englewood Cliffs, NJ: Prentice Hall, 1974, p. 310–327.

Zhang Y, Narayan S, Geiman E, Lanuza GM, Velasquez T, Shanks B, Akay T, Dyck J, Pearson K, Gosgnach S, Fan CM, Goulding M. V3 spinal neurons establish a robust and balanced locomotor rhythm during walking. *Neuron* 60: 84–96, 2008.

Zhong G, Masino MA, Harris-Warrick RM. Persistent sodium currents participate in fictive locomotion generation in neonatal mouse spinal cord. *J Neurosci* 27: 4507–4518, 2007.

Zhong G, Droho S, Crone S, Dietz S, Kwan AC, Webb WW, Sharma K, Harris-Warrick RM. Electrophysiological characterization of the V2a interneurons and their locomotor-related activity in the neonatal mouse spinal cord. *J Neurosci* 30: 170–182, 2010.

Ziskind-Conhaim L, Wu L, Wiesner EP. Persistent sodium current contributes to induced voltage oscillations in locomotor-related hb9 interneurons in the mouse spinal cord. *J Neurophysiol* 100: 2254–2264, 2008.